Solid Earth

Supplement of

A new seismicity catalogue of the eastern Alps using the temporary Swath-D network

Laurens Jan Hofman et al.

Correspondence to: Laurens Jan Hofman (rens@geophysik.fu-berlin.de)

S1.1 Lassie waveform-based event detection

Figure S1 shows a seismic event detection using Pyrocko's Lassie detector (Heimann et al., 2017). This event was detected within the Dolomite indenter (at $11.57°$ E | $46.76°$ N) and could not be linked to any event from any of the public catalogues. Because the Dolomite indenter and the Tauern window have relatively low seismicity rates, the public networks have fewer permanent recording stations in these areas. Therefore, these areas benefit most from the deployment of the Swath-D network. This example shows that it is possible to detect new events using fully automated methods based on the Swath-D data, demonstrating an increased resolution in this part of the area.
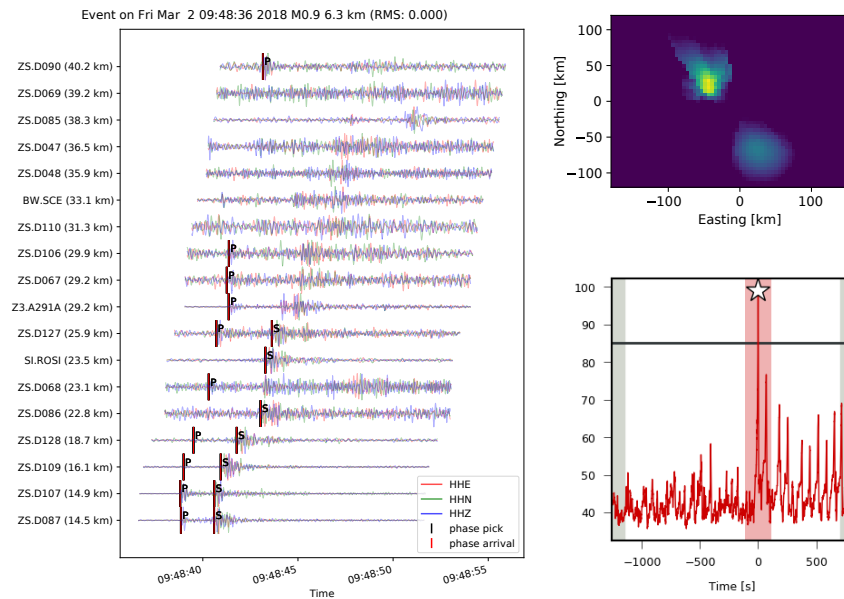

Figure S1. Example of a seismic event detected using Lassie (Heimann et al., 2017). The event is located within the Dolomite indenter at $11.57°$ E | $46.76°$ N at a depth of $6.3\,km$ and occurred on March 2nd, 2018 at $9:48:36$ AM UTC. The left panel shows the event waveforms, sorted by hypocentral distance. The upper right panel shows the image function in space, the lower right panel shows the characteristic function in time.

S1.2   Illustration & examples of cluster-based P & S arrival time picking

The methods used for phase-picking of the detected seismicity are explained in Sect. 3.3, but a few additional, illustrative figures are shown in this section. Figure S2 shows an example of our picking method, where a hand-picked phase from a master event is transferred to a detected event using the cross-correlation function, and an STA/LTA filter. In this example, using only the cross-correlation function (to correlate the hand-picked phase with the expected phase-window of the detected event), would lead to a false pick. The normalisation of the cross-correlation function causes the amplification of noise in the time window before the actual phase arrival. By multiplying the cross-correlation function with the normalised STA/LTA filter, we suppress the pre-arrival noise and ensure that a transient signal is present where we finally set our pick.
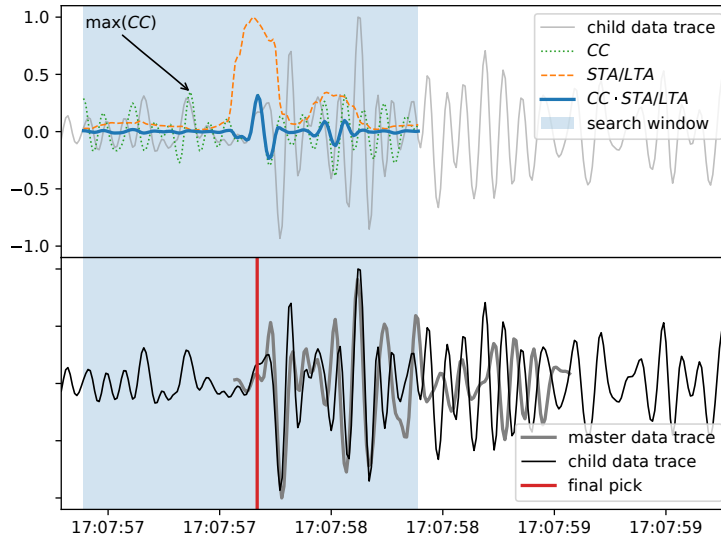

Figure S2. Example of a manual pick transferred to a detected event using the product of the cross-correlation function, and an STA/LTA filter. In this case, using only the cross-correlation would result in a wrong pick. By multiplying both functions, we get a more accurate result. The upper panel shows the cross-correlation function, the STA/LTA filter, and the product of both functions. The lower panel shows the resulting pick and the data trace for the detected event, as well as the master phase used for the cross-correlation.

Another example of our picking method is presented in Fig. S3. This figure shows an example of a master event that is (mainly) hand-picked, and an event detected using that master event that is picked automatically using the methods described in Sect. 3.3.
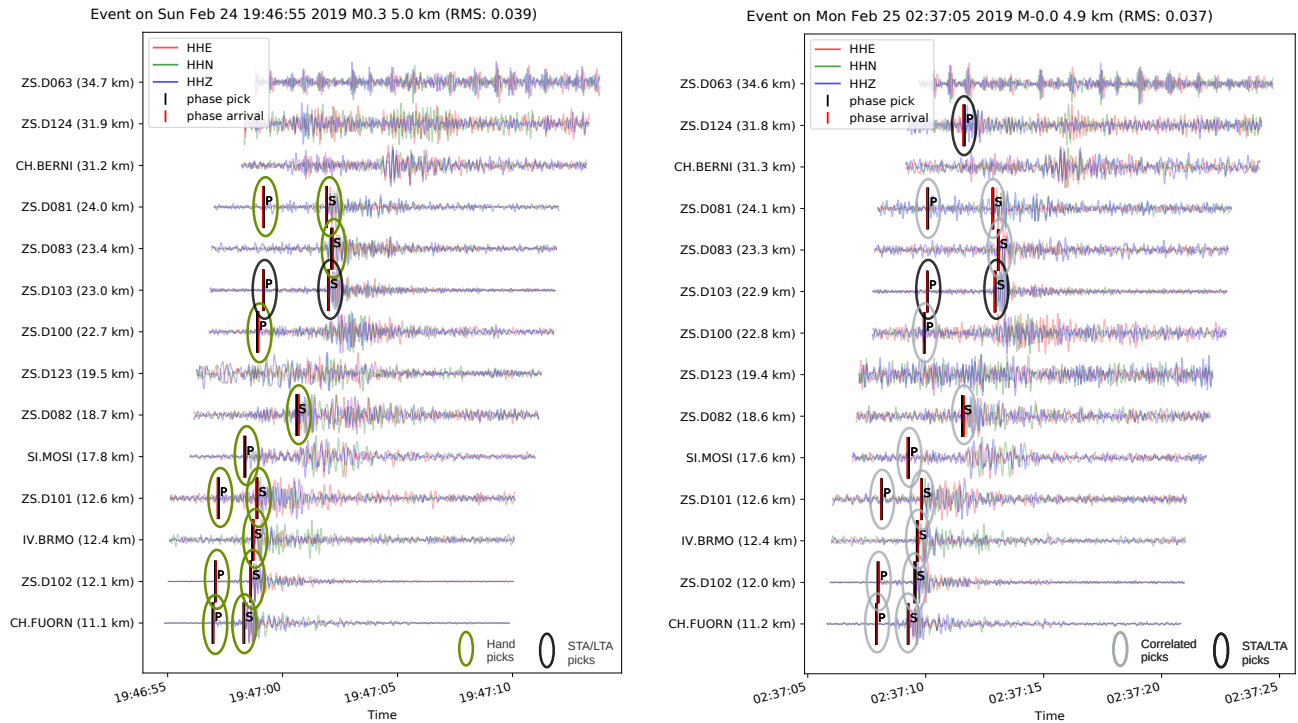
Figure S3. Example of event waveforms for an event used as a template (left panel), and an event that was detected using this template event (right panel). The master event is hand-picked, whereas the picks for the detected event are correlation-based (see Sect. 3.3 for details). Both events contain a few additional STA/LTA picks. The station waveforms are sorted by the hypocentral distance.

S1.3 Arrival time pick optimisation

P- & *S*-arrival time picks for events within each cluster are refined adopting and slightly modifying a method by Shearer (1997). For the N events within a family ($N > 2$), we solve a set of linear equations (equation S1) for the N adjusted arrival times T_i, separately for each phase, either *P*- or *S*-phase, and each station. To avoid numerical problems during the inversion, all time values are taken relative to the event origins.

$$
\begin{pmatrix}
t_1 \\
t_2 \\
t_3 \\
. \\
t_N \\
wcc_{12}\,dt_{12} \\
wcc_{13}\,dt_{13} \\
. \\
wcc_{(N-1)N}\,dt_{(N-1)N}
\end{pmatrix}
=
\begin{pmatrix}
1 & 0 & 0 & . & 0 \\
0 & 1 & 0 & . & 0 \\
0 & 0 & 1 & . & 0 \\
. & . & . & . & . \\
0 & 0 & 0 & . & 1 \\
wcc_{12} & -wcc_{12} & 0 & . & 0 \\
wcc_{13} & 0 & -wcc_{13} & . & 0 \\
. & . & . & . & . \\
0 & 0 & 0 & wcc_{(N-1)N} & -wcc_{(N-1)N}
\end{pmatrix}
\begin{pmatrix}
T_1 \\
T_2 \\
T_3 \\
. \\
T_{N-1} \\
T_N
\end{pmatrix}
\tag{S1}
$$

where t_i are the preliminary time picks relative to the event origin (i.e. travel-time), dt_{ij} are the correlation-based differential travel times (cross-correlation lag time minus the difference in origin times i and j), and wcc_{ij} are weighting factors based on the values of the normalised cross correlation coefficient cc_{ij} for the event pairs (i, j). Here, we use $wcc_{ij} = 1$ if $cc_{ij} > 0.7$ and 0 otherwise. The vector T_i will then contain the updated time picks.

For each event family, station and seismic phase (both *P*- and *S*), we repeat the inversion for a maximum of 15 times, or until the solution converges, and obtain collectively a more consistent set of *P*- & *S*-arrival time picks. The effect of the method is illustrated exemplarily for one event family and one station in Fig. S4.
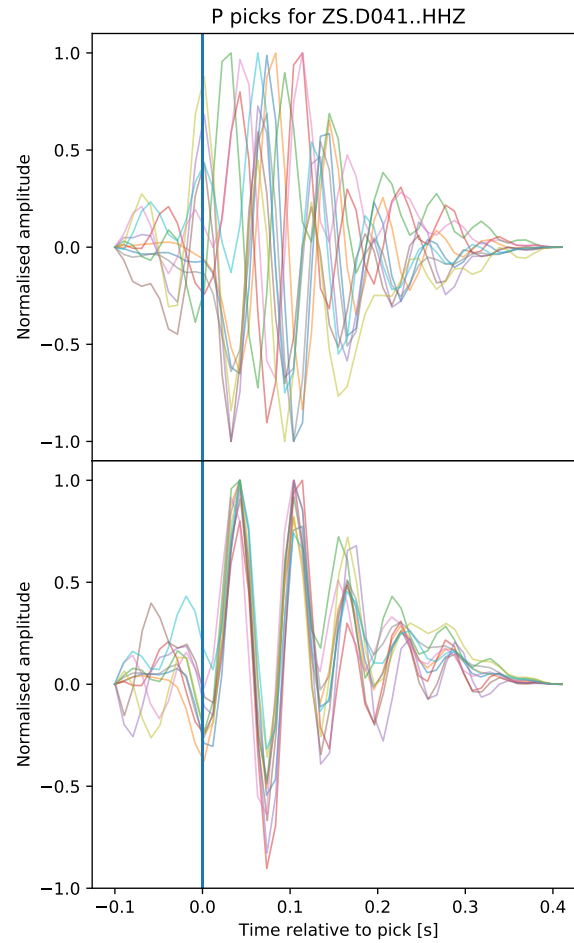
Figure S4. Vertical seismograms for detected events in a template family for one station, aligned on the *P*-pick time before (upper panel) and after (lower panel) applying the method described in Shearer (1997). Note the greatly improved consistency of the phase onsets in the lower panel, equivalent to an improved accuracy of the P- arrival time picks.
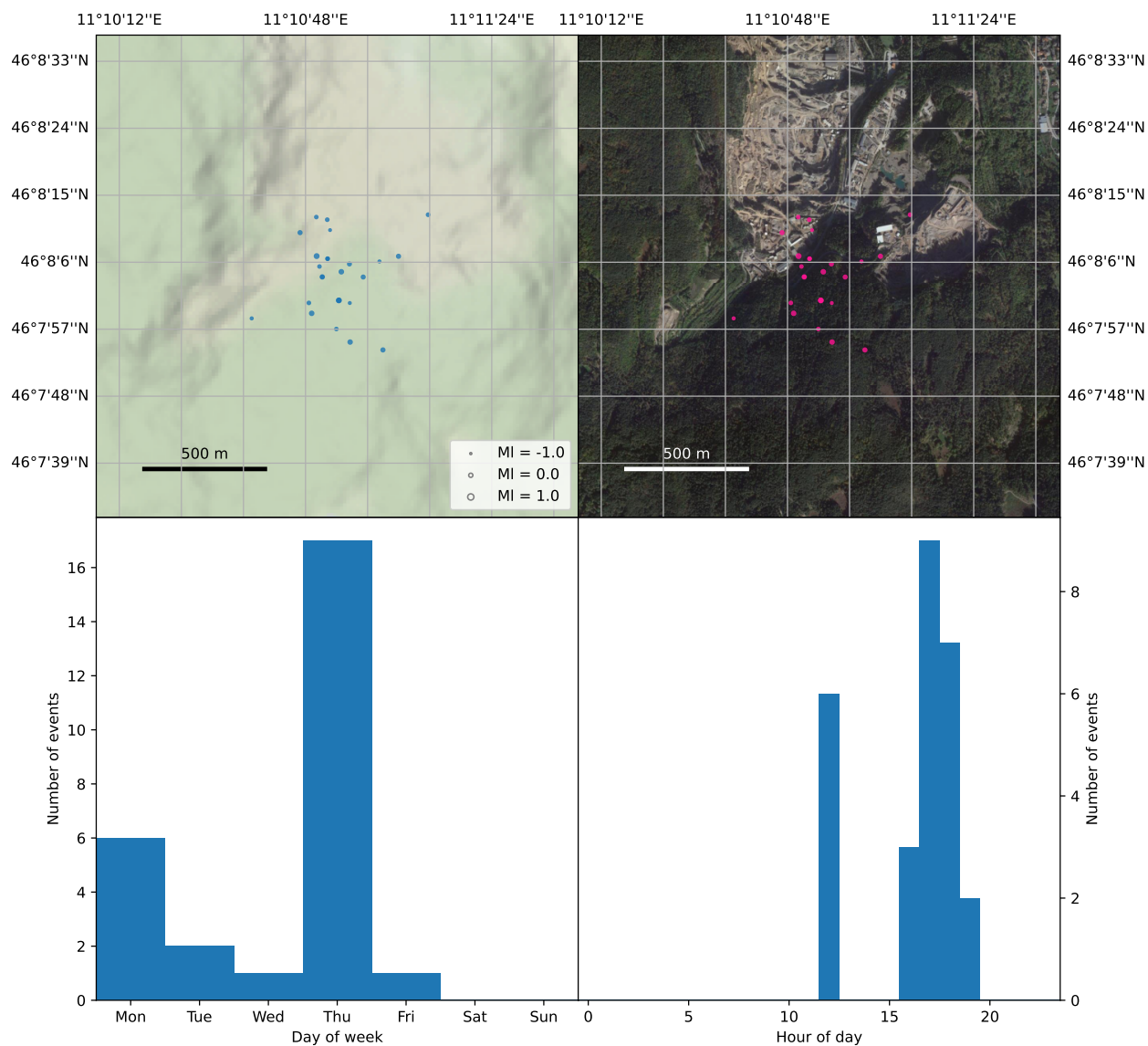
S1.4 Event classification

Figure S5. Example of an event family classified as anthropogenic noise. This figure shows the events from one template family with 27 events (detected using a single master event). The lower panels show the unnatural temporal distribution of the events (only on weekdays, during specific daytime hours). The satellite imagery (top right panel) reveals that the events are located towards the southern end of a large porphyry quarry in the comune of Albiano, Trentino. This is one of the most active quarries in the study area. Map background by Stamen Design [http://stamen.com] under CC BY 3.0. Satellite imagery: Google, ©2023 Maxar Technologies.

S1.5   Calculation of event magnitudes

Event magnitudes are calculated in the local magnitude (M_L) scale (Richter, 1935) using the equation from Bakun and Joyner (1984), given by:

$$M_L = log_{10}(A) + nlog_{10}(R/100) + k(R - 100) + 3 + S \qquad (S2)$$

where A is the geometric mean of the zero-to-peak S-wave amplitudes on the horizontal channels of a simulated Wood-Anderson seismograph in mm, R is the hypocentral distance from source to receiver, n and k are parameters characterising the geometrical spreading and elastic attenuation of S-waves, and S is a station correction term. We adopt the values derived for n and k for northeastern Italy by Bragato and Tento (2005) as shown in Table S1.

Distance [km]	n	k
10-40	1	0.0169
40-80	1	0.0064
80-120	0.5	0.0000
120-170	1	0.0009
170-250	1	0.0027

Table S1. Values for n and k derived for northeastern Italy by Bragato and Tento (2005).

The event magnitude is represented by the median of the individual station magnitudes, where the station correction terms (S) are set to compensate for the mean magnitude residual using the master events.

We observe that the b-value derived from the frequency-magnitude distribution (FMD) (Fig. 6) is significantly lower than 1. This can also be observed in all of the public catalogues we consulted, and indicates that M_l may underestimate the seismic moment. Following Munafò et al. (2016), we estimate the moment magnitudes (M_w) using the scaling relation shown in equation S3. The FMD of the resulting M_w estimates is shown in Fig. S6, yielding a b-value close to one (1.06).
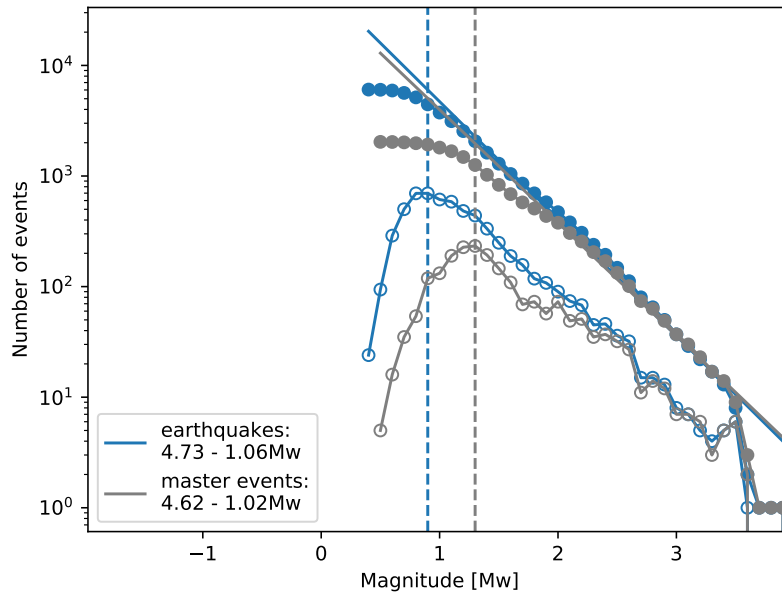
$$M_w = 2/3M_l + 1.5 \qquad (S3)$$

Figure S6. Moment magnitude frequency distribution of the input catalogue (grey) and the final earthquake catalogue (blue) using the scaling relation S3 by Munafò et al. (2016). We obtain the values $a = 4.73$ and $b = 1.06$ for the Gutenberg-Richter relation (Gutenberg and Richter, 1944) using a least-squares fit. The completeness magnitude M_c was estimated at $0.90 M_w$ based on the maximum curvature of the FMD (Wiemer and Wyss, 2000).

Figure S7 shows the relative magnitudes of the detected events in our final catalogue relative to the magnitude of the master events used as templates. It can be clearly observed that the cross-correlation threshold influences the maximum difference in magnitude that can be detected. We use a three-station correlation coefficient (CC) defined as the median of the three highest maximum cross-correlation coefficients on a 10 s window containing the event on the vertical channel. The cross-correlation is performed on 15 stations closest to the event. If a threshold of 0.9 were used, the maximum difference would be restricted to one unit of magnitude, whereas a threshold of 0.5 allows a difference of three units of magnitude. Note that the histogram in Fig. S7 should theoretically be symmetrical. The asymmetry is caused by the skewness of the magnitudes used as master events: the lower magnitude events are underrepresented. This figure therefore shows us that the majority of the detected seismicity is within the range of zero to two units of magnitude lower than the known seismicity in the region.
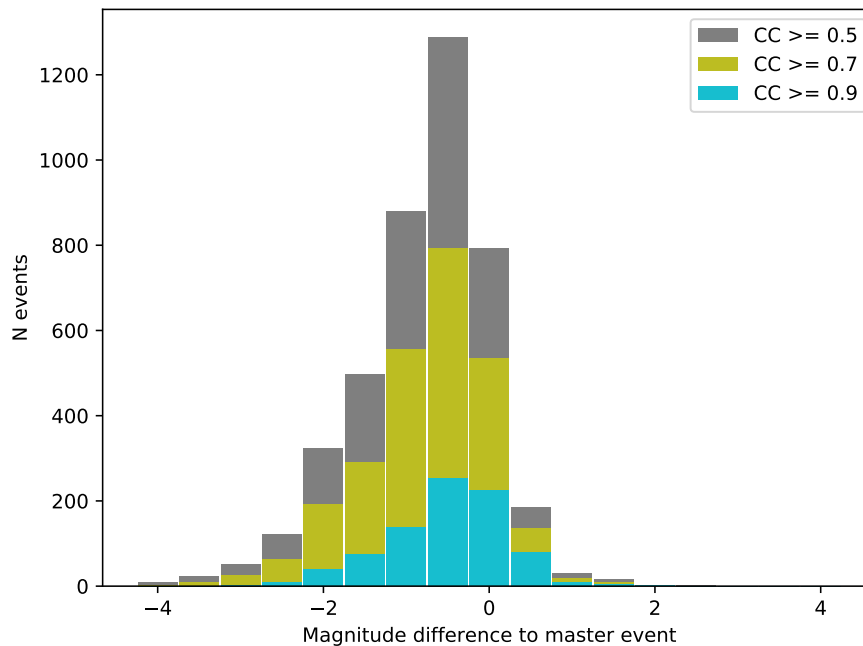

Figure S7. Difference in magnitude δM_L between each event and its master event. The CC values refer to the median of the three highest maximum cross-correlation coefficients, where 15 stations are considered. Each cross-correlation is performed on a 10 s event waveform on the vertical channel.

S1.6 Location uncertainty

This section contains a few additional figures addressing the location uncertainty in our catalogue.
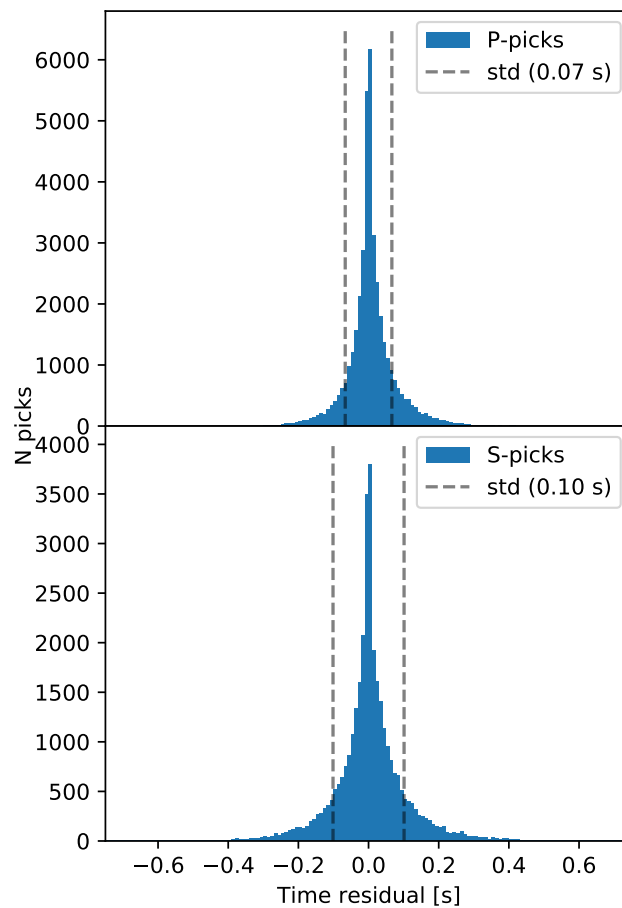

Figure S8. Residuals corresponding to the locations in the final earthquake catalogue for all *P*-picks (upper panel) and *S*-picks (lower panel).
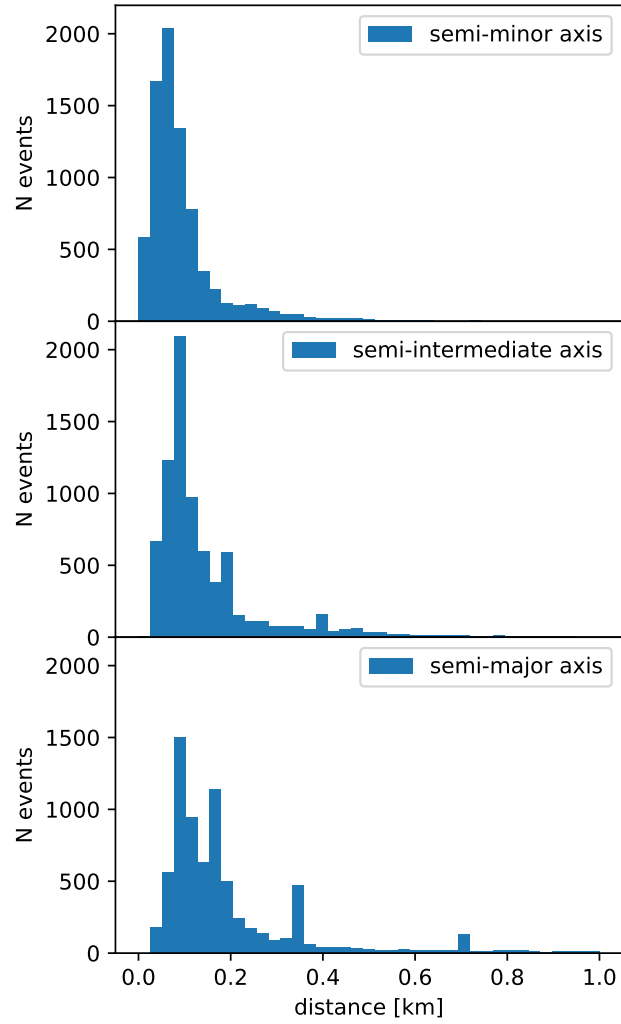
Figure S9. Histograms of the dimensions of the 68% confidence ellipsoids from the hypocenter inversion using NonLinLoc (Lomax et al., 2000).
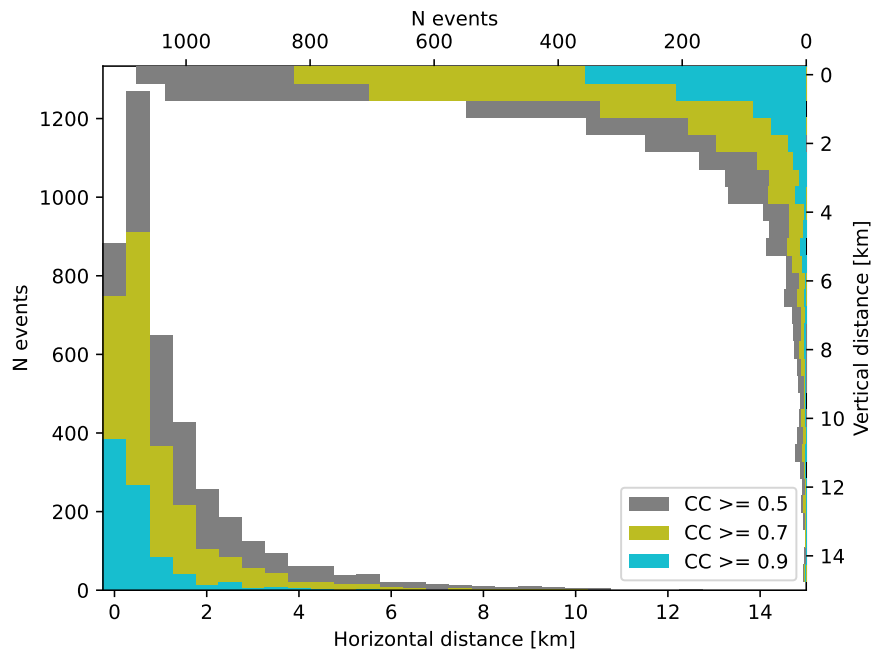
Figure S10. Histograms of the horizontal and vertical distance of the events in the final catalogue with respect to the master events. The CC values refer to the median of the three highest maximum cross-correlation coefficients, where 15 stations are considered. Each cross-correlation is performed on a 10 s event waveform on the vertical channel.
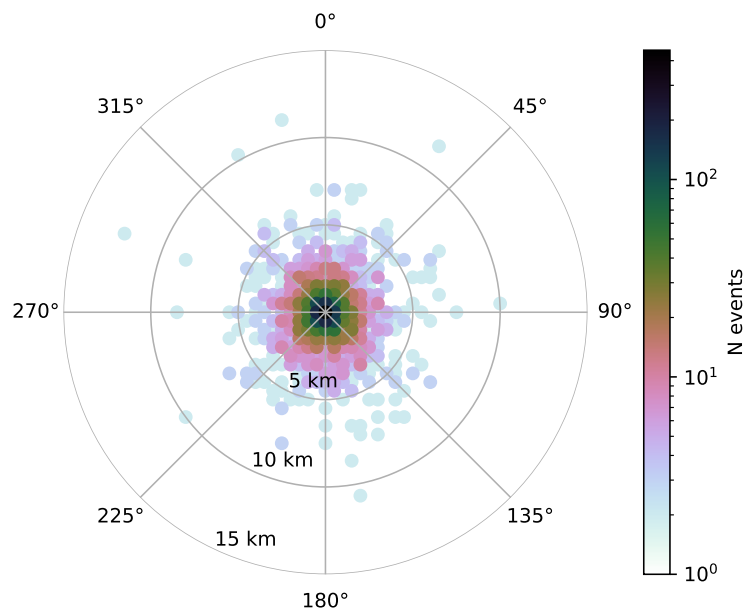
Figure S11. Azimuthal distribution of the events in the final catalogue with respect to the template events. The distances are three-dimensional.
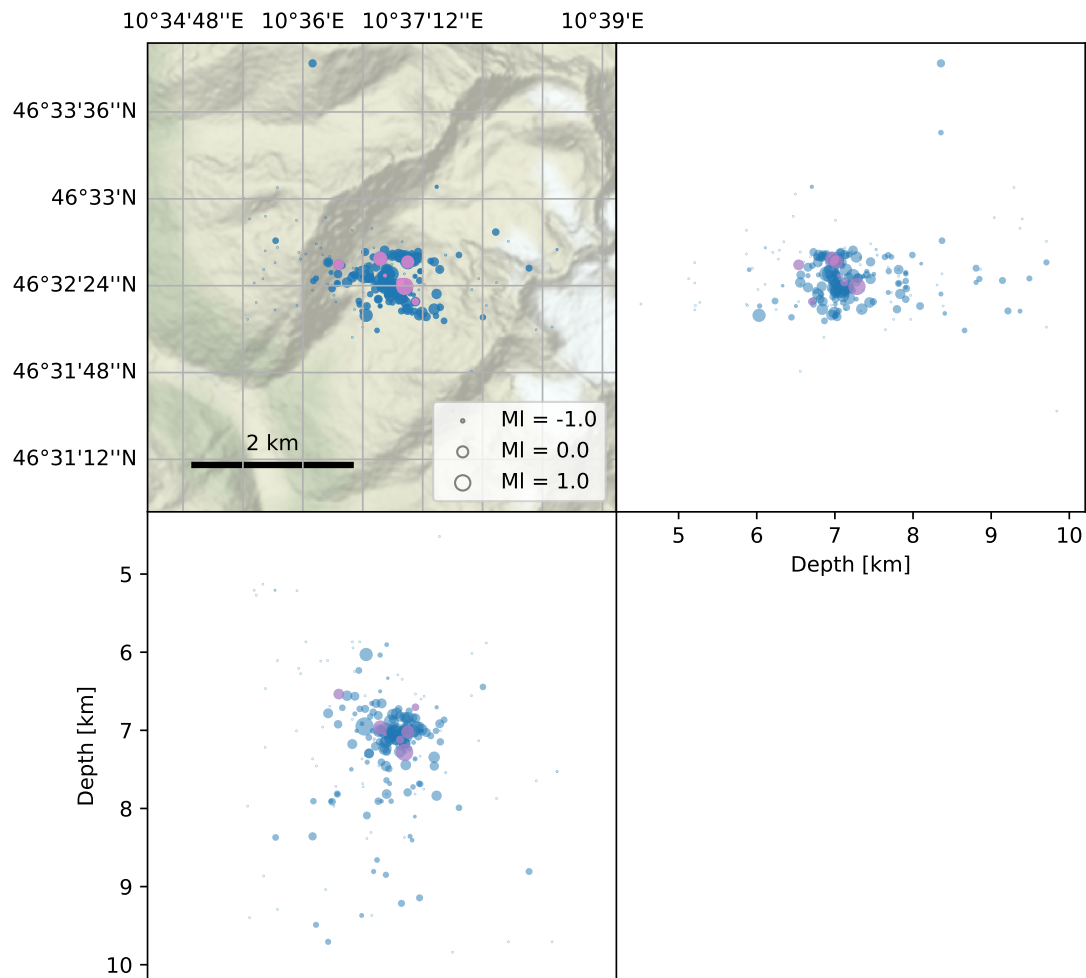
Figure S12. Example of an event cluster consisting of 239 automatically picked and relocated earthquakes (blue circles) based on 7 master events (pink circles). This cluster (marked with the symbol F in Fig. 4 and 7) is located in the Suldental valley on the Swiss-Italian border, and its main sequence took place on February 9th, 2019. Map background by Stamen Design [http://stamen.com] under CC BY 3.0.

References

Bakun, W. H. and Joyner, W. B.: The ML scale in central California, Bulletin of the Seismological Society of America, 74, 1827–1843, 1984.

Bragato, P. L. and Tento, A.: Local magnitude in northeastern Italy, Bulletin of the Seismological Society of America, 95, 579–591, 2005.

Heimann, S., Kriegerowski, M., Isken, M., Cesca, S., Daout, S., Grigoli, F., Juretzek, C., Megies, T., Nooshiri, N., Steinberg, A., Sudhaus, H., Vasyura-Bathke, H., Willey, T., and Dahm, T.: Pyrocko - An open-source seismology toolbox and library, https://doi.org/10.5880/GFZ.2.1.2017.001, 2017.

Lomax, A., Virieux, J., Volant, P., and Berge-Thierry, C.: Probabilistic Earthquake Location in 3D and Layered Models, pp. 101–134, Springer Netherlands, Dordrecht, https://doi.org/10.1007/978-94-015-9536-0_5, 2000.

Munafò, I., Malagnini, L., and Chiaraluce, L.: On the Relationship between Mw and ML for Small Earthquakes, Bulletin of the Seismological Society of America, 106, https://doi.org/10.1785/0120160130, 2016.

Richter, C. F.: An instrumental earthquake magnitude scale, Bulletin of the seismological society of America, 25, 1–32, 1935.

Shearer, P. M.: Improving local earthquake locations using the L1 norm and waveform cross correlation: Application to the Whittier Narrows, California, aftershock sequence, Journal of Geophysical Research: Solid Earth, 102, 8269–8283, 1997.

Wiemer, S. and Wyss, M.: Minimum magnitude of completeness in earthquake catalogs: Examples from Alaska, the western United States, and Japan, Bulletin of the Seismological Society of America, 90, 859–869, 2000.